Keywords: Magnetic materials,Magnetic switching,Magneto optic devices,Magneto optic effects,Optical fiber communication,Optical fiber networks,Optical materials,Optical switches

APPLICATION NOTE 6128

ALL-OPTICAL SWITCHING IN TRANSPARENT NETWORKS: CHALLENGES AND NEW IMPLEMENTATIONS

By: Jin-Wei Tioh, Member of Technical Staff, Maxim Integrated

Abstract: Over the past decade, the influx of high-bandwidth applications has driven a paradigm shift from connection-oriented communications to high-bandwidth IP-centric data traffic. This shift highlighted the need for transparent networks that are bit-rate, protocol, and format insensitive. As these modern networks continue to evolve in both size and complexity, new technologies have emerged to facilitate the most basic networking functions: routing, switching, and multiplexing. This article reviews the state of the art for optical switching, as well as the trends and needs for high-speed switching in optical networks. Some of the latest developments in all-optical switches by the Iowa State University's High-speed Systems Engineering program are also presented and discussed.

Introduction

John Donne stated in 1623 that "No man is an island, entire of itself..." in **Devotions Upon Emergent Occasions**, Meditation XVII. Human beings do not thrive when isolated; thus, his sermon underscores the immense importance of communication. It is also no surprise that optical communication dates back to antiquity, from fire and smoke signals to signaling lamps, flags, and semaphores.

Modern optical communications emerged with the development of both a powerful coherent optical source that could be modulated (lasers[1]) and a suitable transmission medium (optical fibers[2]). Expressed in terms of analog bandwidth, a 1nm waveband translates to a bandwidth of 178GHz at 1300nm and 133GHz at 1500nm. Thus, optical fibers have a total usable bandwidth of approximately 30THz. Assuming the ubiquitous on-off keying format which has a theoretical bandwidth efficiency of 1bps/Hz, one can expect a 30Tbps digital bandwidth if fiber nonidealities are ignored.

Given the immense potential of optical fibers, it comes as no surprise that they are predominantly replacing copper as the transmission medium of choice, vastly increasing single-link bandwidth in the process. As shown in **Figure 1**, the past decade has witnessed a networking paradigm shift from connection-oriented communication to high-bandwidth IP-centric, packet-switched data traffic. All this traffic is driven by the influx of high-bandwidth applications[3] which have caused an insatiable demand for increased data rates in optical long-haul communications.[4] The availability of such high-bandwidth applications relies heavily upon the ability to transport data in a fast and reliable manner without significantly increasing operating and ownership costs. Consequently, researchers are being forced to create high-speed networks capable of supporting the varied bit rates, protocols, and formats required by these applications in a highly scalable manner. As modern networks continue to evolve in both size and complexity, new technologies have emerged to facilitate the most basic networking functions and to efficiently utilize the potential of optical fibers for routing, switching and multiplexing.

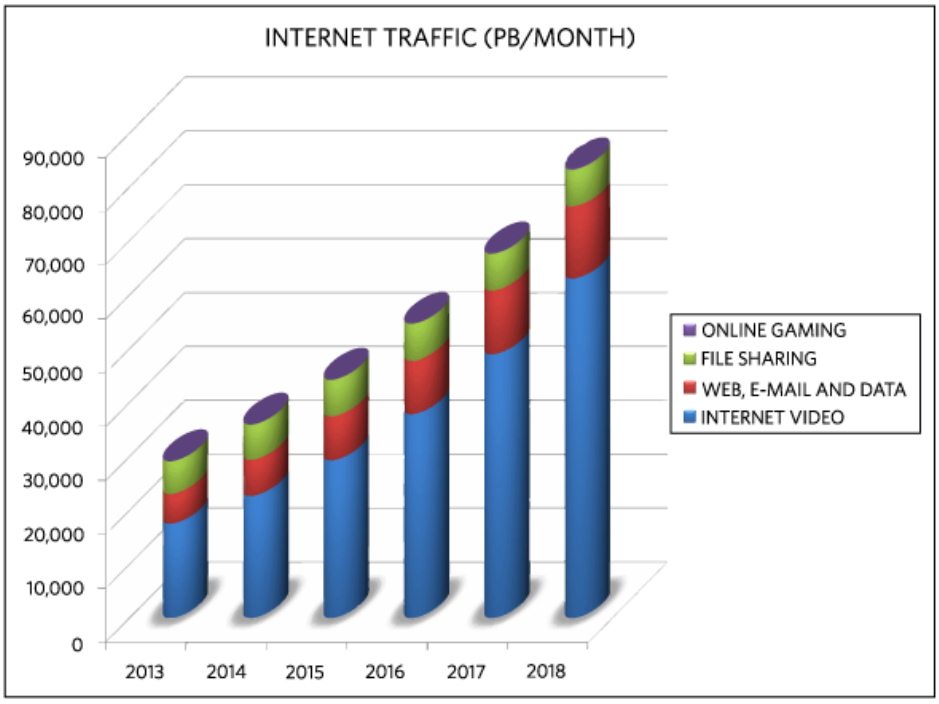

Figure 1. Forecasted growth of global IP traffic. Data source is Cisco report," Cisco Visual Networking Index: Forecast and Methodology 2013-2018." [3]

Transparency

One can define network transparency based on the parameters of the physical layer (e.g., bandwidth, signal-to-noise ratio). It can also be the measurement of the signals remaining in the optical domain, as opposed to those interchanging between the optical and electronic domains. Transparency can also mean the type of signals that the system supports, including modulation formats and bit rates. Given all these considerations, a transparent, all-optical network (AON) is commonly defined as one where the signal remains in the optical domain throughout the network. Transparent networks are attractive due to their flexibility and higher data rate. In contrast, a network is considered opaque if it requires its constituent nodes to be aware of the underlying packet format and bit rate.

The lack of transparency is a pressing concern in current networks, as the need to handle data streams in the electrical domain engenders a large optical-electronic bandwidth mismatch.[5] The bandwidth on a single wavelength is 10Gbps (OC-192/STM-64) today and is likely to exceed 100Gbps (OC-3072/STM-1024) in the near future. Electronics will be hard pressed to keep pace with the optical data rate as it spirals upwards, especially since device dimensions are fast approaching the quantum limit.[6] Additionally, high-speed electronics require prohibitively expensive infrastructure upgrades. Any network upgrade requires the replacement of all legacy equipment (a "forklift upgrade"), which involves the massive overhaul of the existing infrastructure. AONs, however, avoid this problem as the data rate is only limited by the end-station capabilities. Thus, connection upgrades do not require changes in the core, enabling metro operators to scale their networks to meet customer requirements and enhance their services more easily.

The advancement of device implementation technologies makes it possible to design AONs in which optical signals on an arriving wavelength can be switched to an output link of the same wavelength without conversion to the electronic domain. Signals on these AONs can be of different bit rates and formats, as they are never terminated inside the core network. This bit rate, format, and protocol transparency are vitally important in next-generation optical networks.

Switching Technologies

Optical switches can be broadly classified as either opaque or transparent, depending on their implementation technologies.

Opaque switches, also billed as optical cross-connects (OCXs), convert the incoming optical signals into electrical form. The actual switching is then performed electronically using a switching fabric with the resultant signals converted back to optical form at the output. Conversion to the electrical domain offers several advantages including regeneration, free wavelength translation, and better performance and fault management. However, the presence of optical-electrical-optical (OEO) conversions brings with it the

difficulties associated with nontransparent switches noted above.

Transparent switches, also billed as photonic cross-connects (PCXs), do not perform any OEO conversions. This allows them to function independent of the data type, format or rate, albeit only over a range of wavelengths termed the passband. Viable PCX technologies should demonstrate superiority in switching speed, extinction ratio, scalability, insertion loss (IL), polarization-dependent loss (PDL), crosstalk, and power consumption.

Microelectromechnical systems (MEMS) are a powerful means of implementing optical switches because a MEMS system uniquely integrates optical, mechanical, and electrical components on to a single wafer. MEMS switches use micromirrors that redirect light beams to the desired output port.[7-10] MEMS vary in the actuation mechanism used: electrostatic vs. magnetostatic and latching vs. nonlatching. They can be further categorized into either 2D or 3D MEMS. The 2D switches are easier to control and have more stringent tolerances, but do not scale up as well due to optical loss. The 3D switches alleviate the scalability problem by allowing movement on two axes but, consequently, have much tighter tolerances. MEMS switches tend to suffer from higher ILs due to beam divergence (~3dB), slower switching times (ms), high-actuation voltage/current requirements, and higher power dissipation for nonlatching configurations (~80mW). An example of a 2D MEMS switch is illustrated in **Figure 2**.

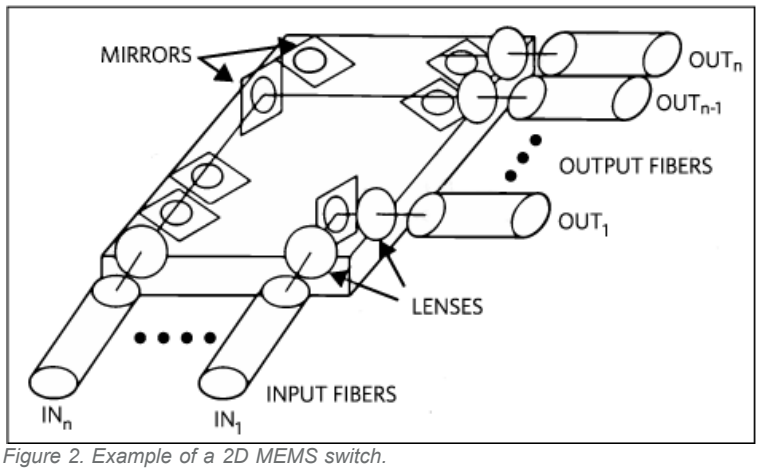

Figure 2. Example of a 2D MEMS switch.

Acousto-optical (AO) switches use ultrasonic waves travelling within a crystal or planar waveguide that deflects light from one path to another,[11-13] as illustrated in **Figure 3**. Mechanical vibration introduces regular zones of compression and tension within a material. In most materials, this compression and tension cause changes in the refractive index. The periodic pattern of refractive index changes then forms a diffraction grating that causes the incoming light to be diffracted. Controlling the ultrasonic wave amplitude and frequency enables control of the amount and wavelength of light that is diffracted. AO switches handle high power levels, offer reasonable IL (~3dB) and switch times (~40µs), but suffer from poor isolation (~-20dB) and power efficiency as well as inherent wavelength dependency.

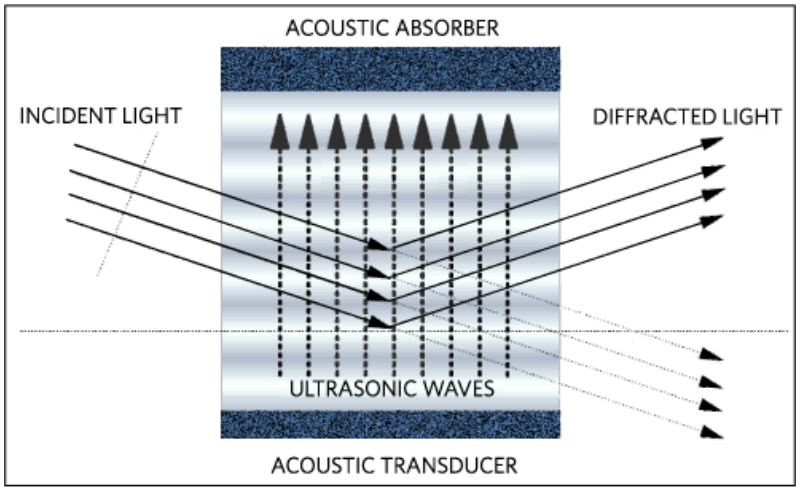

Figure 3. Creation of diffraction grating by ultrasonic waves.

Electro-optical (EO) switches take advantage of the changes in the physical properties of materials when a voltage is applied. These switches have been implemented using liquid crystals, switchable waveguide Bragg gratings, semiconductor optical amplifiers (SOAs), and $LiNbO_3$.[14-18] **Figure 4** shows an EO switch using a $LiNbO_3$ to affect a change in the refractive index of the material that varies linearly with field strength. Depending on the variant, this EO switch offers switching times from 1ns - 1ms; isolations of -10 to -40dB; and ILs ranging from < 1 to 10dB. However, most of these switches have a strong wavelength dependency; those that do not require higher driving voltages.

Semiconductor optical amplifier (SOA)-based switches also suffer from a limited dynamic range, potentially creating cross-modulation and inter-modulation.

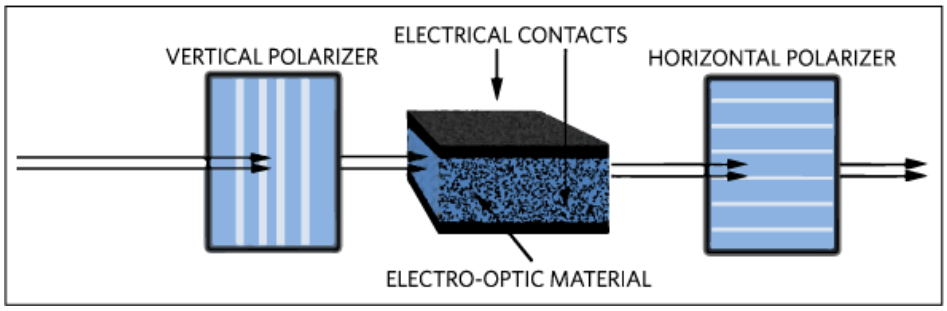

Figure 4. EO switch using LiNbO3 crystal.

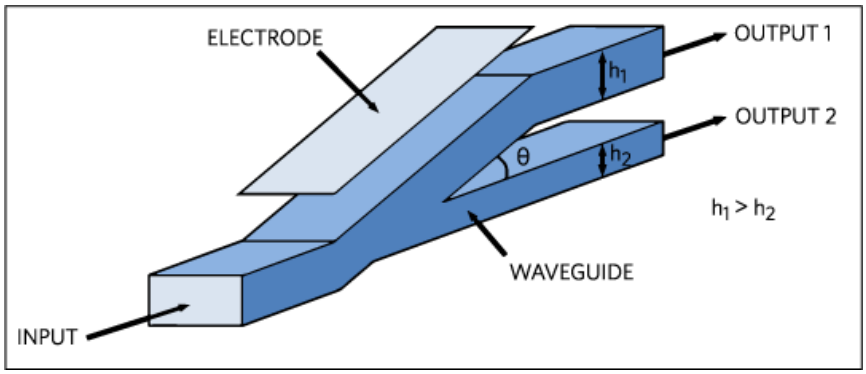

Figure 5. Digital TO waveguide switch.

Thermal-optical (TO) switches are based on either the waveguide thermo-optic effect or the thermal behavior of materials.[19-22] Interferometric TO switches heat the material in one of the interferometer legs to generate a phase shift relative to the other leg. This process leads to interference effects between the two light beams when they are recombined. Digital TO switches utilize the interaction of two silica waveguides on silicon, as shown in **Figure 5**. Heating the material changes the refractive index of the waveguide, imparting a phase difference and, thereby, altering the selectivity of the output ports. While having excellent PDL, digital TO switches consume more power due to the heating process (~70mW) and have slow switch times (ms).

Magneto-optic (MO) switches are based on the Faraday rotation of polarized light when it passes through magneto-optic material in the direction of an applied field.[23] Changing the polarization of an electromagnetic wave is an indirect method of controlling the relative phase of its constituent orthogonal components. One method of achieving this is by exploiting the Faraday effect in a magneto-optic material, i.e., rotating the state of polarization by the Faraday rotation angle θ_F. Magneto-optic switches use an interferometer to convert this phase modulation to an amplitude modulation; these switches hold the distinct advantage of having high-power-handling capability. While some work has previously been done investigating these types of switches[24], the lack of sufficiently high-quality MO materials hampered the effort. Recent advances in bismuth-substituted iron garnets and orthoferrites[25-31] have yielded materials with a high MO figure of merit, giving low ILs, ultrawide bandwidths, and more rotation for less applied fields.

New Implementation and Results

The authors have previously proposed a Mach-Zehnder interferometer (MZI), fiber-based MO switch using a bismuth-substituted iron garnet (BIG) as the Faraday rotator (FR).[32] While showing promising performance and compatibility with contemporary optical network components, that new switch design suffered from a lowered extinction ratio due to unavoidable mismatches in the interferometer paths.

To address the shortcomings of the fiber-based MZI switch, an integrated version was recently proposed and is being actively developed.[33] As a parallel branch of investigation, a Sagnac interferometer configuration is proposed,[34-37] where a BIG FR is placed in the fiber loop, as shown in **Figure 6**. A linearly polarized input wave (E_{1+}) is split by a hybrid coupler into two counter-propagating waves of equal amplitude and 90° out of phase (E_{3-}, E_{4-}). These waves are launched into the Sagnac loop and subsequently encounter the FR. The FR then rotates their polarization by the Faraday rotation angle θ_F that is proportional to the strength of the magnetic field applied to the FR, before arriving back at the coupler (E_{3+}, E_{4+}). Due to the nonreciprocal nature of Faraday rotation, the two counter-propagating waves experience equal and opposite rotations (i.e., θ_F and $-\theta_F$). This action is embodied in (**Eq. 1**) and (**Eq. 2**) using Jones calculus, where E_x and E_y are the x and y components of an incident wave, respectively; T is the transmission coefficient; and φ is the phase change experienced due to the length of the Sagnac loop.

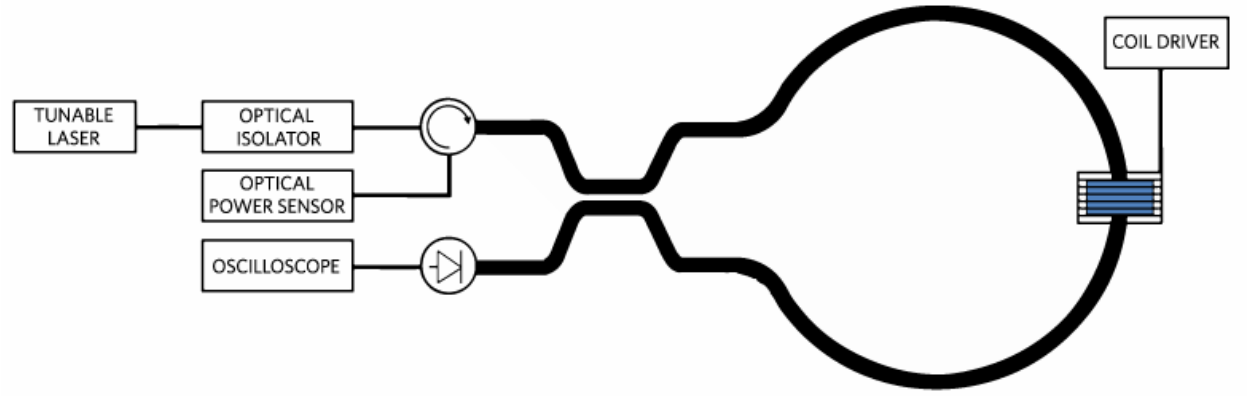

Figure 6. Implementation overview of the Sagnac switch.

Assuming the absence of an input wave at port 2, the outputs at the interferometer ports can be expressed as in (**Eq. 3**). When no field is applied ($\theta_F = 0°$), the input wave is returned to port 1 with a 90° phase shift. Applying a field of sufficient magnitude ($\theta_F = 90°$) redirects the input wave to port 2.

$$\begin{pmatrix} E_{3x+} \\ E_{3y+} \end{pmatrix} = Te^{-j\phi} \begin{pmatrix} \cos\theta_F & \sin\theta_F \\ -\sin\theta_F & \cos\theta_F \end{pmatrix} \begin{pmatrix} E_{4x-} \\ E_{4y-} \end{pmatrix} \quad \text{(Eq. 1)}$$

$$\begin{pmatrix} E_{4x+} \\ E_{4y+} \end{pmatrix} = Te^{-j\phi} \begin{pmatrix} \cos\theta_F & -\sin\theta_F \\ \sin\theta_F & \cos\theta_F \end{pmatrix} \begin{pmatrix} E_{3x-} \\ E_{3y-} \end{pmatrix} \quad \text{(Eq. 2)}$$

$$\begin{pmatrix} E_{1-} \\ E_{2-} \end{pmatrix} = Te^{-j\phi} \begin{pmatrix} (jE_{1x+}\cos\theta_F)\,\hat{x} + (jE_{1y+}\cos\theta_F)\,\hat{y} \\ (-E_{1y+}\sin\theta_F)\,\hat{x} + (E_{1x+}\sin\theta_F)\,\hat{y} \end{pmatrix} \quad \text{(Eq. 3)}$$

Assuming the absence of an input wave at port 2, the outputs at the interferometer ports can be expressed as in (Eq. 3). When no field is applied ($\theta_F = 0°$), the input wave is returned to port 1 with a 90° phase shift. Applying a field of sufficient magnitude ($\theta_F = 90°$) redirects the input wave to port 2.

As shown in **Figure 7**, a switching time of 700ns was achieved with a field intensity of 3.58kA/m. This is markedly better than that of the MZI switch (2μs with 12.7kA/m). However, it can still be improved since, in principle, the achievable switching speed depends on the velocity of the domain walls, which has been measured to be on the order of 10km/s.[38]

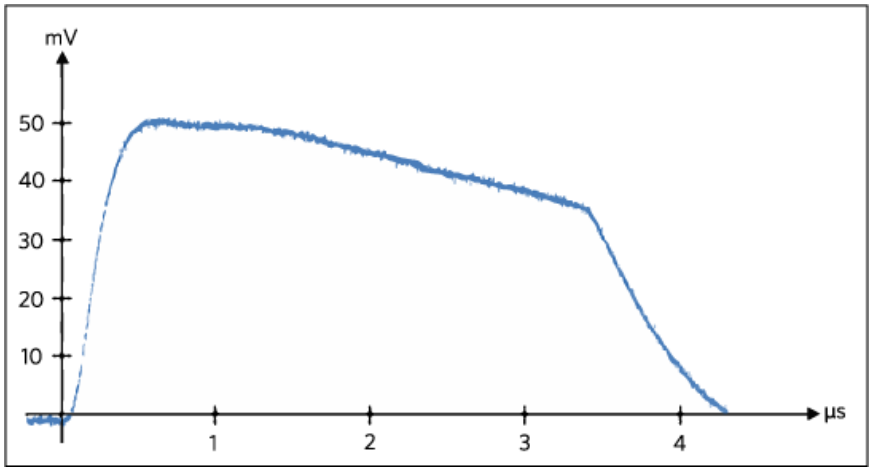

Figure 7. Implementation overview of the Sagnac switch.

Possible approaches to improve switch performance would employ different coil geometries and driver configurations. Both concepts have been recently explored by the authors and show very promising results,[34-36] with risetime reductions to 77ns and falltime reductions to 129ns demonstrated.

Concluding Remarks

An overview of the trends and issues of modern optical communications systems is reported. Transparent network components that perform basic functions (routing, switching, and multiplexing) are the keys to enabling more reliable, scalable, and richly connected optical networks. Some of the latest developments in small-scale, high-speed switching for all-optical lightpath applications are also presented and discussed. Experimental results of the newly implemented switches at Iowa State University are shown.

Bibliography

1. T. H. Maiman, "Stimulated optical radiation in ruby," **Nature**, vol. 187, pp. 493-494, 1960.
2. K. C. Kao, G. A. Hockham, "Dielectric surface waveguide for optical frequencies," **Proc. IEE**, vol. 113, pp. 1151-1158, 1966.
3. Cisco Systems Inc., "Cisco Visual Networking Index: Forecast and Methodology 2013–2018," Jun 2014, www.cisco.com/c/en/us/solutions/collateral/service-provider/ip-ngn-ip-next-generation-network/white_paper_c11-481360.pdf.
4. R. J. Essiambre, R. W. Tkach, "Capacity trends and limits of optical communication networks," **Proc. IEEE**, vol. 100, no. 5, pp. 1035-1055, May 2012.
5. T. Sabapathia, S. Sundaravadivelub, "Analysis of bottlenecks in DWDM fiber optic communication system", **Optik - Intl. J. Light and Electron Optics**, vol. 122, no. 16, pp. 1453-1457, Aug. 2011.
6. J. R. Powell, "The Quantum Limit of Moore's Law," **Proc. IEEE**, vol. 96, no. 8, pp. 1247-1248, Aug. 2008.
7. O. Solgaard, A. A. Godil, R. T. Howe, L. P. Lee, Y. Peter, H. Zappe. "Optical MEMS: From Micromirrors to Complex Systems," J. MEMS, vol. 23, no. 3, pp. 517-538, Jun. 2014.

8. S. Abdulla, L. Kauppinen, M. Dijkstra, E. Berenschot, M. J. de Boer, R. M. de Ridder, G. Krijnen, "Mechano-optical switching in a MEMS integrated photonic crystal slab waveguide," **IEEE Conf. MEMS**, pp. 9-12, Jan. 2011.
9. Q. Chen, W. Wu, H. Mao, B. Du, L. Li, Y. Hao, "Dualfunctional MEMS Optical Device with Compound Electrostatic Actuators for Compact and Flexible Photonic Networks," **IEEE Conf. Sensors**, pp. 2061-2064, Nov. 2010.
10. J. Suzuki, A. Komai, Y. Ohuchi, Y. Tezuka, H. Konishi, M. Nishiyama, Y. Suzuki, S. Owa, "Micro-mirror On Ribbon-actuator (MOR) for high speed spatial light modulator," **IEEE Conf. MEMS**, pp. 762-765, Jan. 2008.
11. G. Aubin, J. Sapriel, V. Molchanov, R. Gabet, P. Grosso, S. Gosselin, Y. Jaouen, "Multichannel acousto-optic cells for fast optical crossconnect," **Electron. Lett.**, vol. 40, pp. 448-449, Apr. 2004.
12. J. Sapriel, D. Charissoux, V. Voloshinov, and V. Molchanov, "Tunable Acoustooptic Filters and Equalizers for WDM Applications," **J. Lightwave Tech.**, vol. 20, no. 5, pp. 892-899, May 2002.
13. H. S. Park, K. Y. Song, S. H. Yun, B. Y. Kim, "All-fiber wavelength tunable acousto-optic switch," **OFC 2001**, vol. 3, pp. 1-3, Mar. 2001.
14. Y. Zhang, Y. Li, S. Feng, A. W. Poon, "Towards Adaptively Tuned Silicon Microring Resonators for Optical Networks-on-Chip Applications," **IEEE J. Sel. Topics Quantum Electron.**, vol. 20, no. 4, Jan. 2014.
15. C. Chen, F. Zhang, H. Wang, X. Sun, F. Wang, Z. Cui, D. Zhang, "UV Curable Electro-Optic Polymer Switch Based on Direct Photodefinition Technique," **IEEE J. Quantum Electron.**, vol. 47, no. 7, pp. 959-964, Jul. 2011.
16. D. Donisi, B. Bellini, R. Beccherelli, R. Asquini, G. Gilardi, M. Trotta, A. d'Alessandro, "A Switchable Liquid-Crystal Optical Channel Waveguide on Silicon," **IEEE J. Quantum Electron.**, vol. 46, no. 5, pp. 762-768, May 2010.
17. Y. Kuratani, M. Kadota, "High-speed and low driving voltage LiNbO3 optical switch composed of new structure," **CLEO**, pp. 1-2, May 2010.
18. W. Wang, Y. Zhao, H. Zhou, Y. Hao, J. Yang, M. Wang, X. Jiang, "CMOS-Compatible 1x3 Silicon Electrooptic Switch with Low Crosstalk," **IEEE Phot. Tech. Lett.**, vol. 23, no. 11, pp. 751-753, Jun. 2011.
19. Q. Zhao, K. Cui, Z. Huang, X. Feng, D. Zhang, F. Liu, W. Zhang, Y. Huang, "Compact Thermo-Optic Switch Based on Tapered W1 Photonic Crystal Waveguide," **IEEE Phot. J.**, vol. 5, no. 2, Apr. 2013.
20. A. M. Al-Hetar, A. B. Mohammad, A. S. M. Supa'at, Z. A. Shamsan, "MMI-MZI Polymer Thermo-Optic Switch With a High Refractive Index Contrast," **J. Lightwave Tech.**, vol. 29, no. 2, pp. 171-178, Jan. 2011.
21. Y. Hashizume, T. Tsuchizawa, T. Watanabe, K. Yamada, S. Itabashi, Y. Nasu, M. Itoh, "Improvement in extinction ratio of silicon-silica hybrid thermooptic switch by using UV laser trimming technique," **OECC**, pp. 80-81, Jul. 2010.
22. T. Zhong, X. M. Zhang, A. Q. Liu, J. Li, C. Lu, D. Y. Tang, "Thermal-Optic Switch by Total Internal Reflection of Micromachined Silicon Prism," **IEEE J. Sel. Topics Quantum Electron.**, vol. 13, no. 2, pp. 348-358, Mar. 2007.
23. J. Tioh, "Interferometric switches for transparent networks: development and integration," 2012, Graduate Theses and Dissertations. Paper 12487, http://lib.dr.iastate.edu/etd/12487/ .
24. Y. S. Didosyan, H. Hauser, G. A. Reider, "Magneto-optic switch based on domain wall motion in orthoferrites," **IEEE Trans. Mag.**, vol. 38, no. 5, pp. 3242–3245, Sep. 2002.
25. M. Bolduc, A. R. Taussig, A. Rajamani, G. F. Dionne, C. A. Ross, "Magnetism and Magnetooptical Effects in Ce-Fe Oxides," **IEEE Trans. Mag.**, vol. 42, no. 10, pp. 3093–3095, Oct. 2006.
26. V. J. Fratello, S. J. Licht, C. D. Brandle, "Innovative improvements in bismuth doped rare-earth iron garnet Faraday rotators," **IEEE Trans. Mag.**, vol. 32, no. 5, pp. 4102– 4107, Sep. 1996.
27. L. Kalandadze, "Influence of Implantation on the Magneto-Optical Properties of Garnet Surface," **IEEE Trans. Mag.**, vol. 44, no. 11, pp. 3293-3295, Nov. 2008.
28. T. Nomura, M. Kishida, N. Hayashi, T. Ishibashi, "Evaluation of Garnet Film as Magneto-Optic Transfer Readout Film," **IEEE Trans. Mag.**, vol. 47, no. 8, pp. 2081–2086, Aug. 2011.
29. K. Shaoying, Y. Shizhuo, V. Adyam, L. Qi, Z. Yong, "Bi3 Fe4Ga1O12 Garnet Properties and Its Application to Ultrafast Switching in the Visible Spectrum," **IEEE Trans. Mag.**, vol. 43, pp. 3656-3660, Sep. 2007.
30. S. Tkachuk, D. Bowen, C. Krafft, I. Mayergoyz, "Controllability of Anisotropy of Bi and Pr Containing Garnet Films Grown on (210)-Oriented Substrates," **IEEE Trans. Mag.**, vol. 44, pp. 3307-3310, Nov. 2008.
31. H. Zhang, Q. Yang, F. Bai, "Microwave/Millimeter-Wave Garnet Films," **IEEE Trans. Mag.**, vol. 47, no. 2, pp. 295-299, Feb. 2011.
32. R. Bahuguna, J. Tioh, M. Mina, R. J. Weber, "Magneto-Optic-Based Fiber Switch for Optical Communications," **IEEE Trans. Mag.**, vol. 42, no. 10, pp. 3099-3101, Oct. 2006.
33. J. Tioh, M. Mina, R. J. Weber, "All-Optical Integrated Switch Utilizing Faraday Rotation," **IEEE Trans. Mag.**, vol. 46, no. 6, pp. 2474–2477, May 2010.
34. J. W. Pritchard, M. Mina, "Magneto-Optic Interferometric Switch with Resonator Configuration," **IEEE Mag. Lett.**, vol. 4, Mar. 2013.
35. J. W. Pritchard, M. Mina, R. J. Weber, "Magnetic Field Generator Design for Magneto-Optic Switching Applications," **IEEE Trans. Mag., vol. 49, no. 7, pp. 4242-4244, Jul 2013.**

36. J. W. Pritchard, M. Mina, R. J. Weber, S. Kemmet, "Low power field generation for magneto-optic fiber-based interferometric switches," **J. Appl. Phys.**, vol. 111, no. 7, pp. 07A941-07A941-3, Mac. 2012.
37. J. Tioh, S. Oster, M. Mina, R. J. Weber, "Optimization of Magneto-optic Device by Low Switching Field Domains," **ISRN Optics**, vol. 2012, pp. 1-5, Jan. 2012.
38. C. H. Tsang, R. M. White, R. L. White, "Transit-time measurements of domain-wall mobilities in YFeO," **J. Appl. Phys.**, vol. 49, no. 12, pp. 6052-6062, Dec. 1978.

A similar version of this article appeared September 16, 2015 on *EDN*.

More Information
For Technical Support: https://www.maximintegrated.com/en/support
For Samples: https://www.maximintegrated.com/en/samples
Other Questions and Comments: https://www.maximintegrated.com/en/contact

---

Application Note 6128: https://www.maximintegrated.com/en/an6128
APPLICATION NOTE 6128, AN6128, AN 6128, APP6128, Appnote6128, Appnote 6128